

AAS 05-338



**OPTIMAL RECONFIGURATION OF A TETRAHEDRAL FORMATION VIA
A GAUSS PSEUDOSPECTRAL METHOD**

Geoffrey T. Huntington and Anil V. Rao

**AAS/AIAA Astrodynamics Specialists
Conference**

Lake Tahoe, CA,

Aug. 7-11, 2005

AAS Publications Office, P.O. Box 28130, San Diego, CA 92198

OPTIMAL RECONFIGURATION OF A TETRAHEDRAL FORMATION VIA A GAUSS PSEUDOSPECTRAL METHOD

Geoffrey T. Huntington* and Anil V. Rao†

This paper addresses the problem of determining a minimum-fuel maneuver sequence to reconfigure a tetrahedral formation. The objective of this work is to develop a single orbit, minimum-fuel reconfiguration strategy such that, after reconfiguration, the four spacecraft are able to return to an acceptable tetrahedral configuration in a region of interest near apogee for a period of three weeks without any required propulsive maneuvers. In the design considered here, an acceptable tetrahedron is obtained by satisfying several constraints on the shape and size of the tetrahedron. The optimal reconfiguration problem is posed as a nonlinear optimal control problem and is solved via direct trajectory optimization using a method called the Gauss pseudospectral method. The results obtained in this study provide insight into the structure of the optimal mission design and demonstrate the generality, computational efficiency, and accuracy of the Gauss pseudospectral method.

1 INTRODUCTION

Spacecraft formation flying is defined as a set of more than one spacecraft whose states are coupled through a common control law.¹ Formation flying has been identified as an enabling technology for many future space missions. In particular, space missions using multiple spacecraft, as compared with using a single spacecraft, allow simultaneous measurements to be taken at specific relative locations, thereby improving science return. An important aspect that is critical to the successful implementation of formation flying missions is trajectory design (also called path planning or guidance²). An excellent survey of methods used to design trajectories for formation flying can be found in Ref. 2. Ref. 2 also provides an extensive list of references on formation flying guidance. Formation flying trajectory design has two main categories: *stationkeeping*, i.e. to maintain a specified relative formation between a cluster of spacecraft for a specified portion of the trajectory and *reconfiguration*, i.e. to maneuver a cluster of spacecraft from one formation to a second formation.

A particular class of Earth-orbit formations that have been studied extensively are those involving four spacecraft.³⁻⁸ Four-spacecraft formations are commonly used because they use relatively few spacecraft while still capable of taking measurements in three-dimensions at relatively large inter-spacecraft distances (e.g. a spacing of several kilometers). However, because of complex mission constraints, it is often difficult to determine feasible trajectories and controls. Because of the already difficult task of determining feasible solutions, it is even more of a challenge to determine solutions that minimize a specified performance metric (e.g. trajectories that minimize fuel). In this research we consider the problem of optimally reconfiguring a four-spacecraft formation from an initial “degraded” formation to a formation that meets a set of mission constraints in a region of the orbit where it is desired to take

*Draper Laboratory Fellow, Guidance and Navigation Division. Ph.D. Candidate, Dept. of Aeronautics and Astronautics, Massachusetts Institute of Technology.

†Senior Member of the Technical Staff, Guidance and Navigation Division, Draper Laboratory, 555 Technology Square, Mail Stop 70, Cambridge, MA 02139.

science measurements. In order to solve this trajectory design problem, the reconfiguration problem is posed as an *optimal control problem*. Moreover, the optimal control problem is nonlinear and has no analytic solutions. Consequently, it is necessary to solve this optimal control problem numerically.

Several papers have attempted to solve tetrahedral formation optimization problems similar to the one considered in this paper. Ref. 9 uses a two-step approach that begins with genetic algorithms and afterwards refines the problem using Lawden's primer vector theory. Ref. 10 also uses a two-step approach, but combines a direct SQP method with a genetic algorithm. Ref. 11 employs a three-step approach that uses simulated annealing as its initial step. In each of these previous works, the problem is separated into pieces where, in general, one piece optimizes the orbital transfer portion of the trajectory and the other piece optimizes the relative position constraints in a sequential but separate optimization procedure that uses the trajectory from the first piece. While dividing the problem into parts and optimizing each part separately makes the problem more tractable, it also reduces the solution search space. Contrariwise, in this work the entire problem is formulated as a *single unified* numerical optimization procedure.

Numerical methods for solving optimal control problems fall into two general categories: indirect methods and direct methods. An excellent survey of various numerical methods for solving optimal control problems can be found in Ref. 12. In an indirect method, the first-order optimality conditions are derived using the minimum principle of Pontryagin.¹³ These necessary conditions lead to a Hamiltonian boundary-value problem (HBVP) which is then solved to determine candidate optimal trajectories called extremal trajectories. In a direct method, the optimal control problem is discretized at specified time points called *collocation points* (common discretization methods used in direct methods include trapezoidal, Hermite-Simpson, and Runge-Kutta¹⁴). The discretized problem is then transcribed to a nonlinear programming problem (NLP) and the NLP is solved using an appropriate optimization method such as those described in Ref. 15 and Ref. 16.

In recent years, direct methods have risen to prominence.^{17,18} The relatively widespread use of direct methods is because direct methods, as compared to indirect methods, are capable of solving a much wider range of complex problems. Furthermore, direct methods are superior to indirect methods in the sense that it is easier to find a solution to the NLP than it is to find a solution to the associated HBVP. Well-known software packages employing direct methods include *Optimal Trajectories by Implicit Simulation* (OTIS),¹⁹ *Sparse Optimal Control Software* (SOCS),²⁰ *Graphical Environment for Simulation and Optimization* (GESOP),²¹ *Direct Collocation* (DIRCOL),²² and *Direct and Indirect Dynamic Optimization* (DIDO).²³

A recently developed class of methods that have shown promise in the numerical solution of optimal control problems are *pseudospectral methods*.²⁴⁻²⁹ In a pseudospectral method, the state and control are approximated using a basis of polynomials.²⁴ Two particular pseudospectral methods that have been previously developed are the *Legendre pseudospectral method*^{25,26} and the *Chebyshev pseudospectral method*.²⁷ It is noted that the Legendre pseudospectral method has been applied to a wide variety of applications including atmospheric entry,³⁰ orbital transfer,³¹ trajectory design for a two spacecraft formation,³² and recently hybrid optimal control.³³

In this research we are interested in applying a newly developed pseudospectral method, called the *Gauss Pseudospectral Method*,³⁴ to the problem of minimum-fuel spacecraft formation reconfiguration. In the Gauss pseudospectral method, the state and control are approximated using a basis of Lagrange interpolating polynomials. The problem is then discretized at a set of points called *Gauss points* (it is noted that the discretization points for the Gauss pseudospectral method differ from discretization points in the Legendre pseudospectral method in that the Legendre pseudospectral method uses *Gauss-Lobatto points*). The Gauss pseudospec-

tral discretization leads to a discrete NLP that can be solved using a variety of well-known optimization algorithms (e.g. SNOPT¹⁶ or SPRNLP¹⁵). Details of the Gauss pseudospectral method are found in Ref. 34.

In this paper, accurate numerical solutions are presented to the problem of single-orbit minimum-fuel spacecraft reconfiguration from a highly degraded initial state to a desired terminal tetrahedron while simultaneously satisfying geometric constraints on the tetrahedron in a region of the orbit near apogee. In addition, trajectories are determined that, even in the presence of disturbances (e.g. sun, moon), maintain the quality of the tetrahedron for a period of three weeks upon exit from the region of interest. All numerical solutions in this research are obtained using the Gauss pseudospectral method of Ref. 34. The optimal trajectories obtained in this study provide insight into the structure of the optimally controlled system, and demonstrate the general applicability of the Gauss pseudospectral method to the problem of optimal spacecraft formation flying trajectory design.

2 SPACECRAFT RECONFIGURATION PROBLEM

Consider a fleet of four spacecraft in Earth orbit near a 1.2×12 Earth radii (R_e) reference orbit with a 10 degree inclination. Furthermore, assume that the initial state of each spacecraft is such that the tetrahedron of the formation is highly degraded and is incapable of being used to take science measurements.⁴ It is desired to reconfigure the four spacecraft into a formation such that the formation satisfies a set of geometric constraints on the tetrahedron for a segment near apogee of the reference orbit. This *region of interest* (ROI) is a segment such that the mesocenter (i.e. the geometric center of the formation) is located a distance greater than $9R_e$ from the center of the Earth (roughly ± 20 deg in true anomaly on either side of apogee).¹ It is known that the initial (degraded) formation does not satisfy the geometric constraints in the region of interest. The problem considered in this paper is to design a single-orbit, minimum-fuel trajectory and control that reconfigures the spacecraft to satisfy both the required geometric constraints in the region of interest and other constraints outside the region of interest. Furthermore, in order to reduce interference with the scientific measurements, it is desired that the spacecraft perform no maneuvers for at least three weeks after the final reconfiguration maneuver. Consequently, the tetrahedron must be able to maintain the specified quality in the region of interest for at least three weeks without additional maneuvers. To assess the quality of the tetrahedron well beyond the final reconfiguration maneuver, the spacecraft are propagated from the terminal state, $\mathbf{x}(t_f)$, of the single orbit minimum-fuel trajectory for a period of three weeks under the influence of several perturbations. The resulting ephemeris of each spacecraft is then used to analyze the tetrahedron during this three-week period to see if the region of interest geometric constraints have been violated. This paper addresses and compares minimum-fuel trajectories that both violate and adhere to this constraint.

3 TRAJECTORY EVENT SEQUENCE

The trajectory event sequence for this problem is given as follows. First, the trajectory is divided into seven phases with the following ordered event sequence:

[Burn Coast Burn Coast Burn Coast ROI]

During the coast phases the thrust is zero, while during the burn phase the thrust is constant at a maximum value T_{\max} . Furthermore, at each phase interface it is assumed that the trajectories and mass of each spacecraft are continuous, but that the control is discontinuous. It

¹The region of interest represents the plasma sheet region of the magnetosphere, in which scientific measurements will be taken.

is important to note that, with the exception of the initial time of each spacecraft in the first phase, the initial and terminal times of *each spacecraft* and *each phase* are free. Also, while no maneuvers are allowed in the region of interest phase (and thus the region of interest phase is a coast phase), several constraints on the formation are applied only in the region of interest. Therefore, the region of interest is specified separately from the other coast phases in the problem. Fig. 1 shows a schematic of the reconfiguration problem.

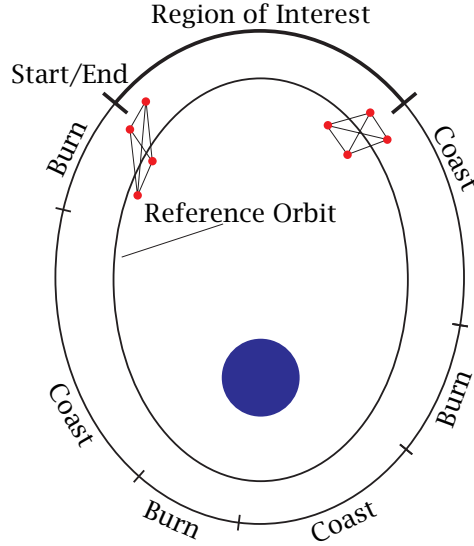


Figure 1: Schematic of Event Sequence for Reconfiguration Problem.

4 SPACECRAFT MODEL AND EQUATIONS OF MOTION

4.1 Spacecraft Model

In this application we consider four identical spacecraft each with a dry mass of 150 kg and a fuel mass of 200 kg. Furthermore, the maximum thrust level of the engine is 0.22 N with an engine specific impulse of 110 s. These physical parameters are typical of a standard mono-propellant hydrazine orbit maintenance thruster.³⁵ Consequently, all thrusting maneuvers are assumed to be non-impulsive. Lastly, there are a few parameters that are not used in the single-orbit optimal control problem, but are used when propagating the spacecraft beyond t_f to analyze the long term effects of the tetrahedral formation under certain perturbations. The drag coefficient, C_d , is 2.2 and the drag area, D_a , is 1 m² for all spacecraft.

4.2 Dynamic Model During Thrust Phases

During all thrust phases the state of each spacecraft is modeled using modified equinoctial elements. The three degree-of-freedom equations of motion for a spacecraft moving over a

spherical nonrotating Earth are given in modified equinoctial elements as³⁶

$$\begin{aligned}
\dot{p} &= \frac{2p}{w} \sqrt{\frac{p}{\mu}} a_\theta \\
\dot{P}_1 &= \sqrt{\frac{p}{\mu}} \left\{ -a_r \cos L + [(w+1) \sin L + P_1] \frac{a_\theta}{w} + [Q_2 \sin L - Q_1 \cos L] \frac{P_2 a_z}{w} \right\} \\
\dot{P}_2 &= \sqrt{\frac{p}{\mu}} \left\{ a_r \sin L + [(w+1) \cos L + P_2] \frac{a_\theta}{w} - [Q_2 \sin L - Q_1 \cos L] \frac{P_1 a_z}{w} \right\} \\
\dot{Q}_1 &= \sqrt{\frac{p}{\mu}} \left(\frac{s^2}{2w} \right) a_z \sin L \\
\dot{Q}_2 &= \sqrt{\frac{p}{\mu}} \left(\frac{s^2}{2w} \right) a_z \cos L \\
\dot{L} &= \sqrt{\mu p} \left(\frac{w}{p} \right)^2 + \sqrt{\frac{p}{\mu}} \frac{Q_2 \sin L - Q_1 \cos L}{w} a_z
\end{aligned} \tag{1}$$

where p is the semi-latus rectum, P_1 , P_2 , Q_1 , and Q_2 have no geometric definition, and L is true longitude. Additionally, $w = p/r = 1 + P_1 \sin L + P_2 \cos L$, $s^2 = 1 + Q_1^2 + Q_2^2$, and a_r , a_θ , and a_z are the perturbing accelerations in the directions of \mathbf{e}_r , \mathbf{e}_θ , and \mathbf{e}_z where \mathbf{e}_r is the unit vector in the radial direction, \mathbf{e}_z is the unit vector in the direction normal to the orbital plane, and $\mathbf{e}_\theta = \mathbf{e}_z \times \mathbf{e}_r$ (thereby completing the right-handed system $\{\mathbf{e}_r, \mathbf{e}_\theta, \mathbf{e}_z\}$). For the application under consideration here, the perturbing accelerations are due entirely to thrust and can be written as

$$a_r = \frac{T}{m} u_r, \quad a_\theta = \frac{T}{m} u_\theta, \quad a_z = \frac{T}{m} u_z, \tag{2}$$

where T is the thrust magnitude, m is the spacecraft mass, and u_r , u_θ , and u_z are the \mathbf{e}_r , \mathbf{e}_θ , and \mathbf{e}_z components, respectively, of the thrust direction. Finally, the mass flow rate of the engine is governed by the equation

$$\dot{m} = -\frac{T}{g_0 I_{sp}} \tag{3}$$

where g_0 is the sea level acceleration due to gravity and I_{sp} is the specific impulse of the engine.

4.3 Dynamic Model for Coast Phases

Since we are assuming a spherical Earth gravity model, during a coast phase the only component of the state that changes with time is the true longitude, L . Consequently, it is possible to model a coast phase much more simply than a thrust phase. In particular, during a coast phase the differential equation for the true longitude can be written as

$$\dot{L} = \frac{dL}{dt} = \frac{\sqrt{\mu p}}{p^2} (1 + P_1 \sin L + P_2 \cos L)^2 = f(L, p, P_1, P_2) \tag{4}$$

Observing that all quantities except L in Eq. (4) are constant, we can separate variables in Eq. (4) to give

$$dt = \frac{dL}{f(L, p, P_1, P_2)} \tag{5}$$

Integrating both sides of Eq. (5), we obtain

$$t_f - t_0 = \int_{L_0}^{L_f} \frac{dL}{f(L, p, P_1, P_2)} \tag{6}$$

where t_0 and t_f are the initial and terminal time, respectively, of the coast phase while $L(t_0) = L_0$ and $L(t_f) = L_f$ are the initial and terminal true longitude, respectively, of the coast phase. Since all other states are constant during a coast phase (again, since we have assumed spherical gravity), the dynamic model for each spacecraft during a coast phase is given as

$$t_f - t_0 - \int_{L_0}^{L_f} \frac{1}{f(L, p, P_1, P_2)} dL = 0, \quad i = 1, \dots, 4 \quad (7)$$

Furthermore, during a coast phase, all other components of the state (i.e. p, P_1, P_2, Q_1, Q_2 , and m) are treated as constant optimization parameters during a coast phase. Finally, it is noted that, due to additional constraints, the above model is not used for the region of interest phase.

5 CONSTRAINTS

5.1 Initial Conditions

As mentioned earlier, the four spacecraft begin in a significantly degraded tetrahedron, shortly after having departed from the region of interest. Table 5.1 shows the initial conditions for each spacecraft in orbital elements. To be clear, a is the semi-major axis in m , e is

Table 1: Spacecraft Initial Conditions

SC num	a_0	e_0	i_0	Ω_0	ω_0	ν_0
1	4.2255510e7	.8025552	.1753710	6.259796	1.6225498	3.5779493
2	4.2255523e7	.8024699	.1753933	6.259694	1.6227984	3.5779235
3	4.2259621e7	.8024827	.1754062	6.260461	1.6217395	3.5781680
4	4.2259623e7	.8254586	.1753016	6.260448	1.6218584	3.5779821

the eccentricity, i is the inclination, Ω is the longitude of the ascending node, ω is the argument of perigee, and ν is the true anomaly. All angle units are in radians. Figure 2 depicts this initial tetrahedron, which shows that this configuration is not the desired regular tetrahedron.

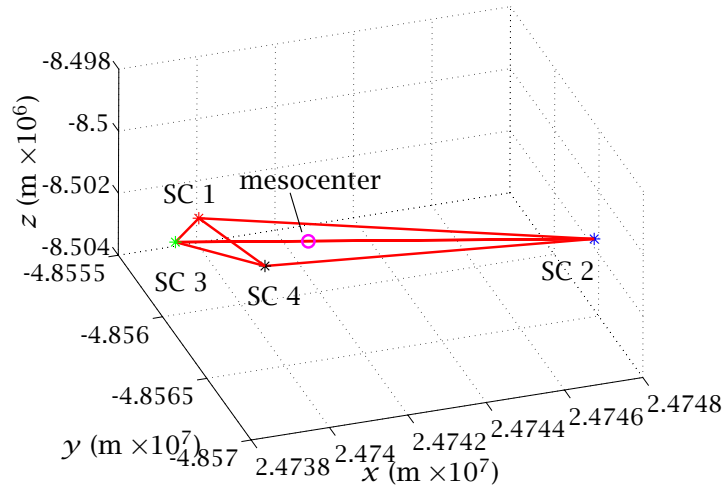


Figure 2: Initial Tetrahedral Configuration.

The orbital elements in Table 5.1 are converted to modified equinoctial elements using a transformation T_{o2e} (see for example Ref. 36) to obtain the initial state in modified equinoctial

elements. Furthermore, the initial mass of each spacecraft is set to its maximum value, i.e.

$$m^{(i)}(t_0) = m_{max}, \quad i = 1, \dots, 4 \quad (8)$$

where for this problem, $m_{max} = 350$ kg.

5.2 Interior Point Constraints

As stated earlier, in order for the trajectory to be continuous at each phase interface, it is necessary to enforce linkage conditions at every phase boundary. These linkage conditions are enforced on the modified equinoctial elements, mass, and time and are given as follows:

$$\begin{aligned} p^{(i)}(t_f^{(j)}) &= p^{(i)}(t_0^{(j+1)}), & P_1^{(i)}(t_f^{(j)}) &= P_1^{(i)}(t_0^{(j+1)}) \\ P_2^{(i)}(t_f^{(j)}) &= P_2^{(i)}(t_0^{(j+1)}), & Q_1^{(i)}(t_f^{(j)}) &= Q_1^{(i)}(t_0^{(j+1)}) \\ Q_2^{(i)}(t_f^{(j)}) &= Q_2^{(i)}(t_0^{(j+1)}), & L^{(i)}(t_f^{(j)}) &= L^{(i)}(t_0^{(j+1)}) \\ m^{(i)}(t_f^{(j)}) &= m^{(i)}(t_0^{(j+1)}), & t_f^{(i)(j)} &= t_0^{(i)(j+1)} \end{aligned} \quad i = 1, \dots, 4 \quad j = 1, \dots, P-1 \quad (9)$$

where i is the i^{th} spacecraft, j is the j^{th} phase and P is the number of phases in the problem under consideration (in this case $P = 7$). Finally, in order to ensure that time is increasing during the trajectory, the following inequality constraints are placed on the time during each phase of the trajectory:

$$t_f^{(i)(j)} - t_0^{(i)(j)} \geq 0, \quad i = 1, \dots, 4, \quad j = 1, \dots, P \quad (10)$$

5.3 Trajectory Path Constraints during Thrust Phases

During a thrust phase, the following path constraints are imposed on the four spacecraft. First, it is necessary to constrain the thrust direction to be unit length. Defining the thrust direction as $\mathbf{u}_T = [u_r \quad u_\theta \quad u_z]^T$, the following constraint is imposed on \mathbf{u}_T during the thrust phases:

$$\mathbf{u}_T \cdot \mathbf{u}_T = 1 \quad (11)$$

Second, the mass of each spacecraft cannot fall below the vehicle dry mass. Defining the dry mass of each vehicle as m_{dry} , the following inequality constraint is imposed on the mass of each spacecraft during the each phase of the trajectory:

$$m^{(i)} \geq m_{dry}, \quad i = 1, \dots, 4 \quad (12)$$

5.4 Constraints in the Region of Interest Phase

The final phase of the trajectory spans the region of interest. In the region of interest, several geometric constraints are placed on the formation. As noted in Section 3, this phase is a coast phase. Consequently, the thrust is zero in the region of interest. Next, let the spacecraft *mesocenter* (i.e. the mean position) be defined as

$$\bar{\mathbf{r}} = \frac{1}{4} \sum_{i=1}^4 \mathbf{r}^{(i)} \quad (13)$$

where $\mathbf{r}^{(i)}$, $i = 1, \dots, 4$ are the positions of the four spacecraft as measured from the center of the Earth. At the start of the region of interest phase, the mesocenter must attain a particular position on the reference orbit, \mathbf{r}_{ROI} , where $\|\mathbf{r}_{ROI}\| = 9R_e$ and is located at a point prior to

apogee. Consequently, a constraint on the position of the mesocenter at the start of the region of interest is given as

$$\bar{\mathbf{r}}(t_0^{(P)}) = \mathbf{r}_{ROI} \quad (14)$$

A second constraint enforced at the entrance of the region of interest is as follows. In the absence of perturbations, a spacecraft's orbit period is solely a function of semi-major axis. Consequently, a formation in which all spacecraft have equal semi-major axes will be periodic in its motion. When perturbations are introduced, there will be some degradation to the tetrahedron over time, but in general the degradation rate is reduced if the orbit periods are equal at the start. Therefore, in order for the formation to maintain its quality in the ROI for a period of time into the future (i.e. beyond t_f), it is beneficial to require that the semi-major axes of each spacecraft at the start of the region of interest. Applying this condition, a second constraint on the formation in the region of interest is given as

$$\mathbf{a}^{(1)}(t_0^{(P)}) = \mathbf{a}^{(2)}(t_0^{(P)}) = \mathbf{a}^{(3)}(t_0^{(P)}) = \mathbf{a}^{(4)}(t_0^{(P)}) \quad (15)$$

Now, the region of interest terminates when the position of the mesocenter has again attained a magnitude of $9R_e$. Consequently, a constraint at the terminus of the region of interest is given as

$$||\bar{\mathbf{r}}(t_f^{(P)})|| = 9R_e \quad (16)$$

Next, several path constraints are enforced during the region of interest. First, as the formation evolves in the region of interest, it must maintain a certain geometry in order to be able to take useful scientific measurements. In particular, the two aspects to the formation geometry that are important in order to fulfill the science requirements are the *shape* and *size* of the formation. The metric used to determine the quality of the shape of the formation is the Glassmeier metric (Q_{gm}).³⁷ The Glassmeier metric is given as

$$Q_{gm} = \frac{V_a}{V^*} + \frac{SA_a}{SA^*} + 1 \quad (17)$$

where V_a is the actual volume of the tetrahedron, SA_a is the actual surface area of the tetrahedron, and V^* and SA^* are the volume and surface area, respectively, of a regular tetrahedron whose average side length is \bar{L} . It is noted that the largest possible value of each ratio in Eq. (17) is unity. Consequently, the maximum value of Q_{gm} is 3. It is seen that the Glassmeier quality metric is a function of both volume and surface area of the tetrahedron. However, because of the functional form of Q_{gm} , the Glassmeier metric has no sensitivity to the size of the tetrahedron. The ideal geometry for this mission is a regular tetrahedron with 10 km spacing between each satellite, but science investigators note that there is considerable flexibility here.⁴ In particular, values of Q_{gm} greater than 2.7 are acceptable in the region of interest. Consequently, the following path constraint on Q_{gm} is enforced in the region of interest

$$Q_{gm} \geq 2.7 \quad (18)$$

See Appendix for the computation of the Glassmeier quality factor.

Because the Glassmeier metric is insensitive to the size of the tetrahedron, an additional constraint is required to constrain the size of the tetrahedron. Although an average inter-spacecraft separation of 10 km is considered ideal, acceptable science return is still possible for average separations ranging from 4 km to 18 km.⁴ Consequently, the following path constraint is enforced during the region of interest that keeps the average side length, \bar{L} , bounded between its acceptable lower and upper limits:

$$4 \leq \bar{L} \leq 18. \quad (19)$$

Next, in order to evaluate the aforementioned path constraints in the region of interest at the same time for all four spacecraft, it is necessary that both the initial and terminal time for all four spacecraft be the same. Constraints on the initial and terminal time in the region of interest are then given as

$$\begin{aligned} t_0^{(1)(P)} &= t_0^{(2)(P)} = t_0^{(3)(P)} = t_0^{(4)(P)} \\ t_f^{(1)(P)} &= t_f^{(2)(P)} = t_f^{(3)(P)} = t_f^{(4)(P)} \end{aligned} \quad (20)$$

It is noted that t_0 and t_f in these equations are *free*.

5.5 Dynamic Model in Region of Interest

Because the path constraints in the region of interest are based on Cartesian Earth-centered inertial (ECI) position and velocity, it is simpler to use a dynamic model in the region of interest that is consistent with the mathematical form of the region of interest constraints. Consequently, as opposed to modified equinoctial elements, the dynamics of each spacecraft in the region of interest phase are described using ECI position and velocity. The dynamic model used during the region of interest phase is then given as

$$\dot{\mathbf{r}} = \mathbf{v}, \quad \dot{\mathbf{v}} = -\frac{\mu}{r^3} \mathbf{r} \quad (21)$$

In order to maintain continuity between the phases, the Cartesian variables are transformed to modified equinoctial elements at the start of the region of interest phase and are set equal to the elements at the final time of the previous phase (similar to Eq. (9)).

6 OPTIMAL CONTROL PROBLEM IN BOLZA FORM

Consider the following general optimal control problem.^{38,39} Determine the state $\mathbf{x}(t) \in \mathbb{R}^n$, control $\mathbf{u}(t) \in \mathbb{R}^m$, and final time t_f , that minimize the Bolza cost functional

$$J = \Phi(\mathbf{x}(t_f), t_f) + \int_{t_0}^{t_f} g(\mathbf{x}(t), \mathbf{u}(t), t) dt \quad (22)$$

subject to the differential dynamic constraints,

$$\dot{\mathbf{x}}(t) = \mathbf{f}(\mathbf{x}(t), \mathbf{u}(t), t), \quad t \in [t_0, t_f] \quad (23)$$

the boundary conditions

$$\boldsymbol{\phi}(\mathbf{x}(t_0), t_0, \mathbf{x}(t_f), t_f) = \mathbf{0} \quad (24)$$

and equality state and control constraints enforced as path constraints

$$\mathbf{C}(\mathbf{x}(t), \mathbf{u}(t), t) = \mathbf{0}, \quad t \in [t_0, t_f] \quad (25)$$

In Eqs. (22)-(25), the functions Φ , g , f , ϕ , and C are defined as follows:

$$\begin{aligned} \Phi &: \mathbb{R}^n \times \mathbb{R} \rightarrow \mathbb{R} \\ g &: \mathbb{R}^n \times \mathbb{R}^m \times \mathbb{R} \rightarrow \mathbb{R} \\ \mathbf{f} &: \mathbb{R}^n \times \mathbb{R}^m \times \mathbb{R} \rightarrow \mathbb{R}^n \\ \boldsymbol{\phi} &: \mathbb{R}^n \times \mathbb{R} \times \mathbb{R}^n \times \mathbb{R} \rightarrow \mathbb{R}^q \\ \mathbf{C} &: \mathbb{R}^n \times \mathbb{R}^m \times \mathbb{R} \rightarrow \mathbb{R}^c \end{aligned} \quad (26)$$

The problem of Eqs. (22)-(25) will be referred to as the continuous Bolza problem.

7 OPTIMAL TETRAHEDRAL RECONFIGURATION PROBLEM

The optimal control tetrahedral reconfiguration problem is now stated formally. Using the aforementioned trajectory event sequence, determine the thrust profile that maximizes the sum of the terminal masses of each spacecraft, i.e. maximize the objective functional

$$J = \sum_{i=1}^4 m^{(i)}(t_f^{(P)}) \quad (27)$$

subject to the dynamic constraints of Eq. (1), (3), and (7), the initial constraints of Table 5.1 and Eq. (8), the interior point constraints of Eq. (9) and (10), the path constraints of Eq. (11) and (12), the terminal constraints of Eq. (14), (15), (16), (20), (17), and (19).

8 GAUSS PSEUDOSPECTRAL METHOD

The Bolza problem is defined on the time interval $t \in [t_0, t_f]$. However, in order to apply the Gauss pseudospectral method,³⁴ the time interval $t \in [t_0, t_f]$ must be transformed to the time interval $\tau \in [-1, 1]$. The transformation that maps the interval $t \in [t_0, t_f]$ to $\tau \in [-1, 1]$ is given as

$$\tau = \frac{2t - (t_f + t_0)}{t_f - t_0} \quad (28)$$

Using Eq. (28), the cost functional of Eq. (22) is then given in terms of τ as

$$J = \Phi(\mathbf{x}(1), t_f) + \frac{t_f - t_0}{2} \int_{-1}^1 g(\mathbf{x}(\tau), \mathbf{u}(\tau), \tau) d\tau \quad (29)$$

Similarly, the dynamic constraints of Eq. (23), the boundary conditions of Eq. (24) and path constraints of Eq. (25) are given in terms of $\tau \in [-1, 1]$ as

$$\frac{2}{t_f - t_0} \frac{d\mathbf{x}}{d\tau} = \mathbf{f}(\mathbf{x}(\tau), \mathbf{u}(\tau), \tau), \quad (30)$$

$$\boldsymbol{\phi}(\mathbf{x}(-1), t_0, \mathbf{x}(1), t_f) = \mathbf{0}, \quad (31)$$

$$\mathbf{C}(\mathbf{x}(\tau), \mathbf{u}(\tau), \tau) = \mathbf{0} \quad (32)$$

The continuous Bolza problem is now be approximated pseudospectrally by approximating the state $\mathbf{x}(\tau)$, by a polynomial, $\mathbf{X}(\tau) \in \mathbb{R}^n$. This polynomial approximation is formed using a basis of $N + 1$ Lagrange interpolating polynomials, $L_0(\tau), \dots, L_N(\tau)$, on the interval from $[-1, 1]$ as

$$\mathbf{x}(\tau) \approx \mathbf{X}(\tau) = \sum_{i=0}^N \mathbf{x}(\tau_i) L_i(\tau) \quad (33)$$

where $L_i(\tau)$, ($i = 1, \dots, n$) is the i^{th} Lagrange polynomial and is defined as

$$L_i(\tau) = \prod_{j=0, j \neq i}^N \frac{(\tau - \tau_j)}{(\tau_i - \tau_j)} \quad (34)$$

It is known that $L_i(\tau)$ has the property that

$$L_i(\tau_j) = \delta_{ij} = \begin{cases} 1 & i = j \\ 0 & i \neq j \end{cases}, \quad i, j = 0, \dots, N \quad (35)$$

The interpolation points used here are the initial point, ($\tau_0 = -1$), along with the N Gauss points where the Gauss points lie on the interior of the interval $[-1, 1]$. The derivative of the state approximation in Eq. (33) is collocated at the N Gauss points as follows:³⁴

$$\left[\frac{d\mathbf{x}}{d\tau} \right]_{\tau_k} \approx \left[\frac{d\mathbf{X}}{d\tau} \right]_{\tau_k} = \sum_{i=0}^N \mathbf{X}(\tau_i) \left(\frac{dL_i}{d\tau} \right)_{\tau_k} = \sum_{i=0}^N D_{ki} \mathbf{X}(\tau_i) = \mathbf{f}(\mathbf{X}(\tau_k), \mathbf{U}(\tau_k), \tau_k), \quad k = 1 \dots N \quad (36)$$

where D_{ki} are elements in the $D \in \mathbb{R}^{N \times (N+1)}$ *Differentiation Matrix*. For clarity, this matrix is divided into two submatrices. The first column of D , corresponding to the initial point, τ_0 , is isolated and denoted as $\bar{D} \in \mathbb{R}^N$, where $\bar{D}_k = \dot{L}_0(\tau_k)$. The remaining part of D , denoted $\tilde{D} \in \mathbb{R}^{N \times N}$, corresponds to the collocation at the Gauss points. It is known that $\tilde{D}_{ki} = \dot{L}_i(\tau_k)$. The approximation to the derivative of the state at the Gauss points is then given as

$$\left[\frac{d\mathbf{x}}{d\tau} \right]_{\tau_k} = \dot{\mathbf{x}}(\tau_k) \approx \dot{\mathbf{X}}(\tau_k) = \bar{D}_k \mathbf{X}(\tau_0) + \sum_{i=1}^N \tilde{D}_{ki} \mathbf{X}(\tau_i), \quad k = 1 \dots N \quad (37)$$

The continuous-time optimal control problem is now transcribed to a nonlinear programming problem (NLP) using the variables $\mathbf{X}_k = \mathbf{X}(\tau_k) \in \mathbb{R}^n$ for the state and $\mathbf{U}_k = \mathbf{U}(\tau_k) \in \mathbb{R}^m$ for the control at the k^{th} Gauss point, where $k = 1, \dots, N$. The initial and final states, $\mathbf{X}_0 = \mathbf{X}(\tau_0) \in \mathbb{R}^n$ and $\mathbf{X}_f = \mathbf{X}(\tau_f) \in \mathbb{R}^n$, respectively, are also included as variables in the NLP, for a total of $N + 2$ *nodes*. Note that when using the Gauss Pseudospectral method, the differential dynamic constraints are applied only at the N collocation points whereas the state is approximated at $N + 1$ interpolation points (including $\tau_0 = -1$). See Ref. 34 for more details.

In this NLP, the cost functional in Eq. (29) is approximated using a Gauss quadrature as

$$J = \Phi(\mathbf{X}_f, t_f) + \frac{(t_f - t_0)}{2} \sum_{k=1}^N w_k g(\mathbf{X}_k, \mathbf{U}_k, \tau_k) \quad (38)$$

where w_k are the Gauss weights. The discretized differential dynamic constraints, boundary constraints, and control path constraints of Eq. (30) (collocated at Gauss points) are given as

$$\bar{D}_k \mathbf{X}_0 + \sum_{i=1}^N \tilde{D}_{ki} \mathbf{X}_i = \frac{t_f - t_0}{2} \mathbf{f}(\mathbf{X}_k, \mathbf{U}_k, \tau_k), \quad k = 1, \dots, N \quad (39)$$

In addition to the dynamic constraints, the initial and final state are related via the quadrature

$$\mathbf{X}_f = \mathbf{X}_0 + \frac{t_f - t_0}{2} \sum_{k=1}^N w_k \mathbf{f}(\mathbf{X}_k, \mathbf{U}_k, \tau_k) \quad (40)$$

The discretized boundary conditions of Eq. (31) are expressed in their general form as

$$\boldsymbol{\phi}(\mathbf{X}_0, t_0, \mathbf{X}_f, t_f) = \mathbf{0} \quad (41)$$

Lastly, the discretized control path constraints of Eq. (32) are expressed as follows

$$\mathbf{C}(\mathbf{X}_k, \mathbf{U}_k, \tau_k) \leq \mathbf{0}, \quad k = 1, \dots, N \quad (42)$$

The cost functional of Eq. (38) together with the constraints of Eqs. (39), (40), (41), and (42) define a nonlinear programming problem (NLP). The solution of this NLP is an approximate solution to the continuous-time optimal control problem.

9 NUMERICAL SOLUTION VIA GAUSS PSEUDOSPECTRAL METHOD

The spacecraft configuration problem as described in Section 2 - Section 7 is solved using the aforementioned Gauss pseudospectral method.³⁴ The optimization was carried out with the MATLAB mex interface of the NLP solver SNOPT⁴⁰ using analytic first-order derivatives for both the constraint Jacobian and the gradient of the objective function. Furthermore, the optimal control problem was scaled canonically from SI units to a non-dimensional set of units such that the length scale is the radius of the Earth, the time scale is one Schuler period, and the mass scale is equal to the initial spacecraft mass. For this numerical reconfiguration problem, 10 nodes (i.e. 8 Gauss points) were used for the burn phases, and 50 nodes (i.e. 48 Gauss points) were used in the region of interest coast phase. The coast phases (other than the region of interest phase) were not discretized, but were computed via numerical quadrature of Eq. (7). Consequently, each coast phase had two nodes representing the initial and final points of the phase.

Ideally, science investigators would like the formation geometry constraints to hold while inside the ROI for a period of three weeks. Yet, the problem described in the previous sections has a duration of only one orbit, or roughly one day. Because of this, any constraints on the formation after this first pass through the ROI are not explicitly coded into the problem. However, the solution to the single-orbit problem was propagated for three weeks using an orbit propagation tool called FreeFlyer to determine the effects of perturbations on the formation. These results are presented in the following section. The problem was then solved with a tighter requirement on the tetrahedral formation, which, when propagated for three weeks, met the tetrahedral requirements for the entire duration. The results of this case are presented in the following section as well.

10 RESULTS

10.1 Minimum-Fuel Solution for $Q_{\min} = 2.7$

A minimum-fuel solution to the problem posed in Section 7 with $Q_{\min} = 2.7$ is presented here. The total amount of fuel burned is $\sum_{i=1}^4 m_f^i = 0.1289$ kg. The propellant used by each spacecraft is shown in Fig. 3. Furthermore, Table 2 describes in detail the phase durations for each spacecraft. Although three maneuver opportunities were included in the trajectory design, it is seen in the optimal trajectory that at least one maneuver was of zero duration for each spacecraft. In fact, as seen in Table 2, only spacecraft #4 used more than one of the three provided maneuver opportunities. In addition, all of the thrust maneuvers were relatively short in duration (the longest burn being roughly six minutes in duration). It is also interesting to note that spacecraft #1 burned over half of the total fuel expended and that this maneuver resulted in a significant change in the position of spacecraft #1 relative to the other three spacecraft. By examining the tetrahedral formation at the initial time (Fig. 4) and the tetrahedral formation at the terminal time (Fig. 5), it can be seen that the optimal solution essentially re-positioned spacecraft #1 according to the arrow in Fig. 4, with only minor changes in the other three spacecraft. It is important to note that this optimal trajectory design is unique to the initial conditions given, meaning different initial conditions could result in very different maneuver profiles.

Table 2: Phase Durations (in minutes) for $Q_{\min} = 2.7$.

SC num	Burn1	Coast1	Burn2	Coast2	Burn3	Coast3	Coast ROI
1	0	158.483	0	355.017	6.224	61.533	837.300
2	1.118	226.667	0	164.500	0	188.967	837.300
3	0	157.483	0	84.083	1.746	337.950	837.300
4	0.383	272.717	1.143	75.000	0	232.017	837.300

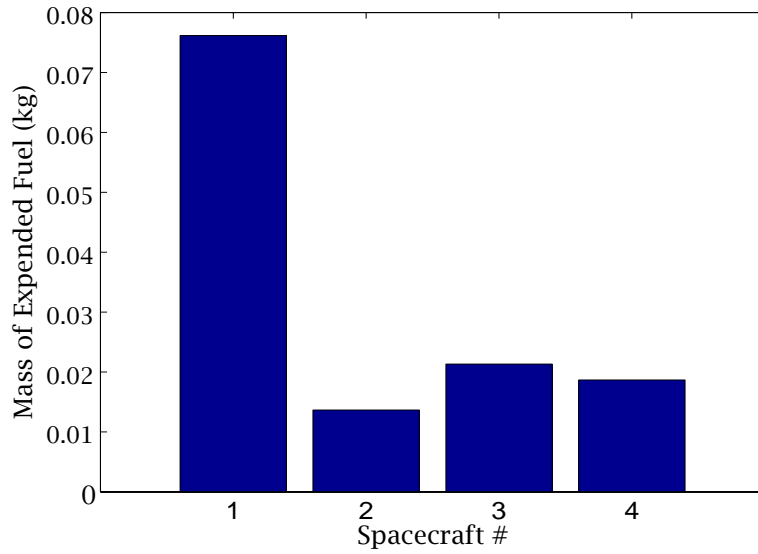


Figure 3: Fuel Expenditure of Each Spacecraft for $Q_{\min} = 2.7$.

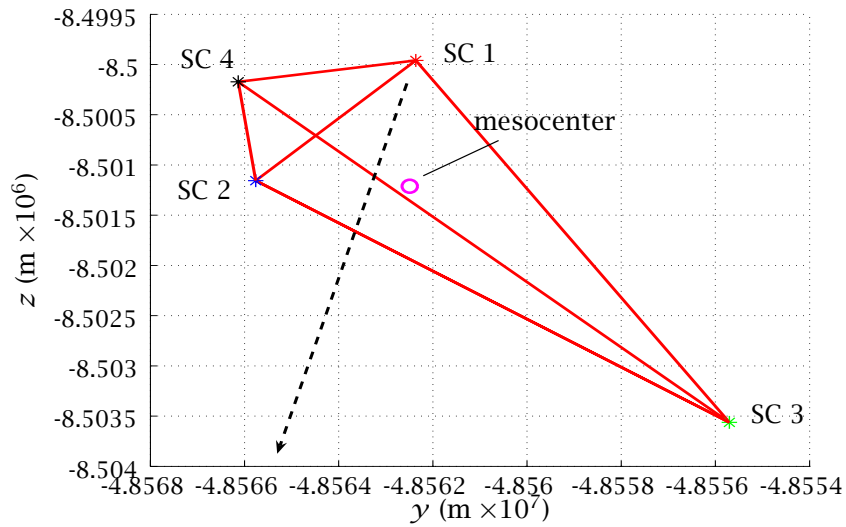


Figure 4: Projection of Initial Tetrahedron into ECI YZ-Plane for $Q_{\min} = 2.7$.

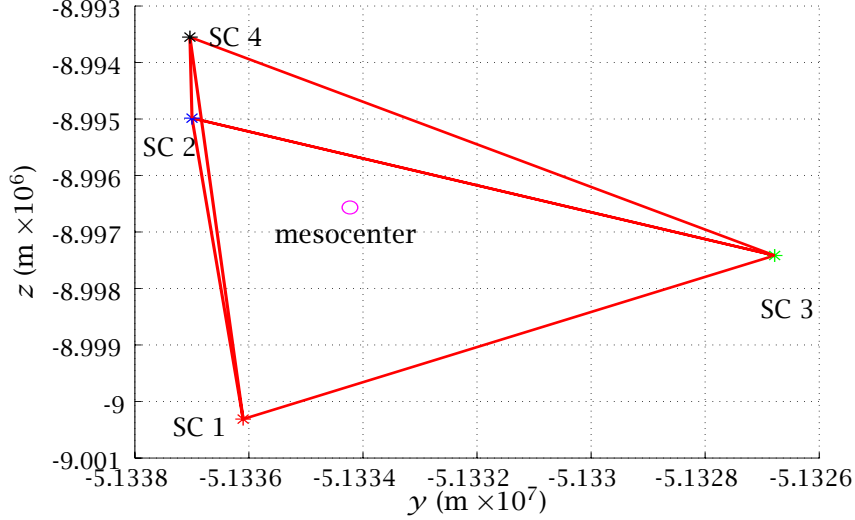


Figure 5: Projection of Terminal Tetrahedron into ECI YZ-Plane for $Q_{\min} = 2.7$.

Fig. 6 shows the evolution of the Glassmeier quality factor, Q_{gm} , in the region of interest. Note that the constraint on the quality factor becomes active twice during the region of interest, once at the terminal point and once in the middle of the region of interest. Interestingly, as seen in Figs. 6 and 7, the instant of time near the middle of the region of interest where the quality factor attains its lower bound occurs when the average length has simultaneously attained its minimum value. When the spacecraft are in close proximity, small changes in relative position can lead to large changes in the relative geometry. As a result, the sensitivity of the shape of the tetrahedron to changes in average length is highest when the spacecraft are more closely spaced. In particular, this sensitivity can result in a rapid degradation of the quality factor. Fig. 8 supports this by showing that the sensitivity of the quality factor with respect to the average length, $\partial Q_{gm} / \partial \bar{L}$, is indeed largest at the time that \bar{L} is at a minimum.

Finally, it is observed from Fig. 7 that the average length always remains between its upper and lower bound in the region of interest. A possible explanation why the average length never attains its lower bound is because of the shape of the tetrahedron is highly sensitive to changes in \bar{L} when the average length is small. As a result, it may be difficult to maintain the quality factor if \bar{L} is too small. A possible explanation as to why the average length never attains its upper bound is that an exceedingly large value of \bar{L} may result in an increase in fuel consumption (since the initial tetrahedron, while deformed, has an acceptable average side length only of 9.054 km). As a result, a tetrahedron with a large average length would not be fuel-optimal.

10.2 Ensuring Future Satisfaction of Quality Factor Constraint

It is important to note that the fuel-optimal solution described in Section 10.1 does not consider any potential degradation in the quality factor beyond a single passage though the region of interest. However, if no more maneuvers were performed after the spacecraft have exited the region of interest, it is clear that perturbations (e.g. oblateness, solar, lunar, and drag) could potentially degrade the quality of the tetrahedron. As a result, at a future time, the quality of the formation would be unacceptable.

As an example of potentially unacceptable degradation in the quality of the formation, sup-

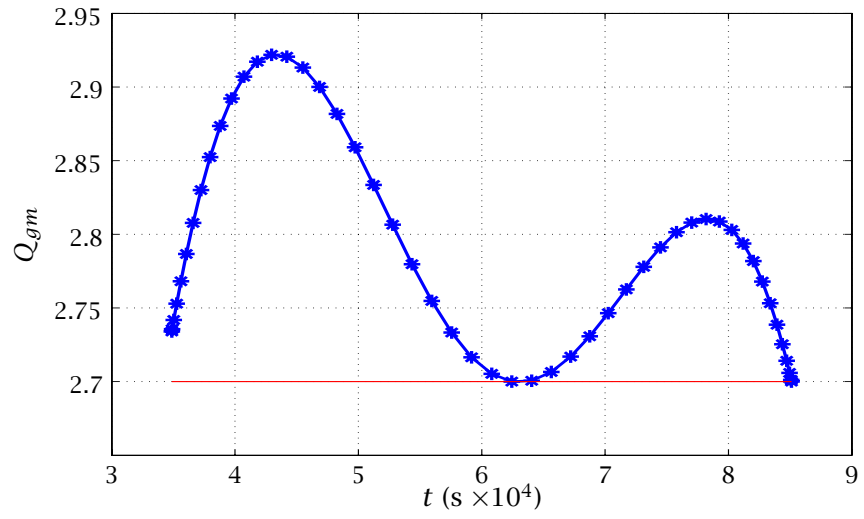


Figure 6: Quality Factor in Region of Interest for $Q_{\min} = 2.7$.

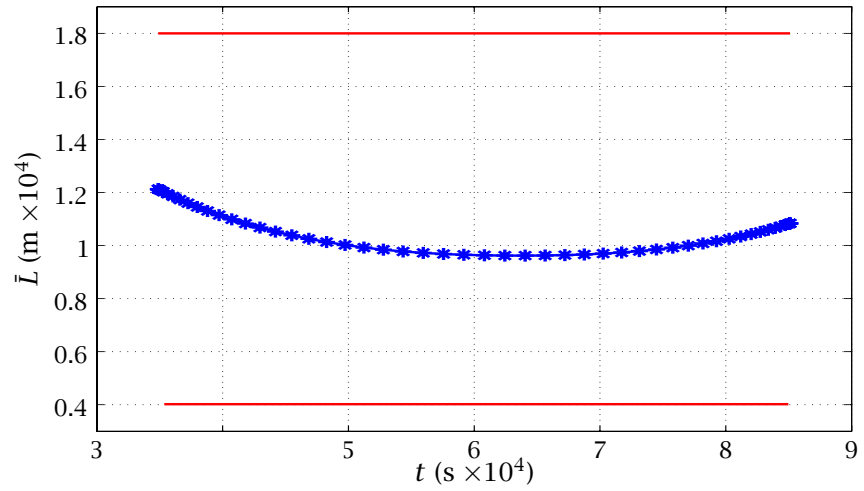


Figure 7: Average Length, \bar{L} , in Region of Interest for $Q_{\min} = 2.7$.

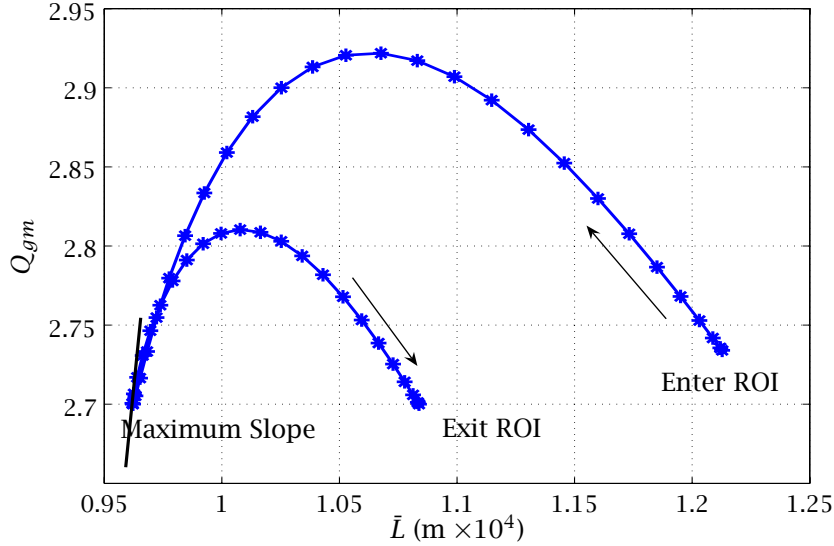


Figure 8: Quality Factor, Q_{gm} , as a Function of Average Length, \bar{L} , in Region of Interest for $Q_{\min} = 2.7$. Note: Slope of Q_{gm} Attains a Maximum When \bar{L} Attains a Minimum.

pose that, upon the first exit from the region of interest, it is required that *no maneuvers* be performed for a period of three weeks in order to take measurements without interruption. Naturally, the tetrahedron must be able to maintain a quality factor of greater than 2.7 during every passage through the region of interest for this three-week period. A question that arises then is whether an optimal trajectory (such as that obtained in Section 10.1) meets these requirements. Fig. 9 shows the trajectory obtained when the final state of the optimal trajectory of Section 10.1 is propagated forward over a period of three weeks.² It is seen from Fig. 9 that the quality of the tetrahedron begins to degrade in the region of interest on subsequent revolutions. More specifically, it is seen in Fig. 9 that, within 20 revolutions (1 revolution \approx 1 day), the quality of the tetrahedral formation no longer satisfies the requirement on the quality factor in the region of interest. However, it is noted that the average side length between the spacecraft changes very little (Fig. 10) over this three-week period, due in large part to the constraint of Eq. 15 on the semi-major axis.

Ideally, the way to ensure that the quality factor constraint is met for a specified time into the future would be to pose an optimal control problem that includes a sufficient number of revolutions of the orbit and enforces the quality factor constraint during the region of interest in every revolution. However, this is computationally cumbersome since the size of the optimal control problem would increase substantially. An alternative to solving such a complex optimal control problem is to include some margin in the quality factor constraint for the single revolution optimal control problem (i.e. the problem considered in this paper). In particular, it may be useful to set the lower bound on Q_{gm} to a value that is higher than the desired value of 2.7 and see if the tetrahedron is of acceptable quality for three-weeks into the future.

In order to demonstrate the effectiveness of providing margin in the quality factor, the original optimal control problem was modified so that the lower limit on Q_{gm} in the first region of interest was 2.8 instead of 2.7. The final state of this modified problem was then propagated for three weeks. The results of this modified problem are shown in Fig. 11. Although the

²The three-week propagation was performed using the orbit propagation tool *FreeFlyer* using oblateness, solar, lunar, and drag perturbations.

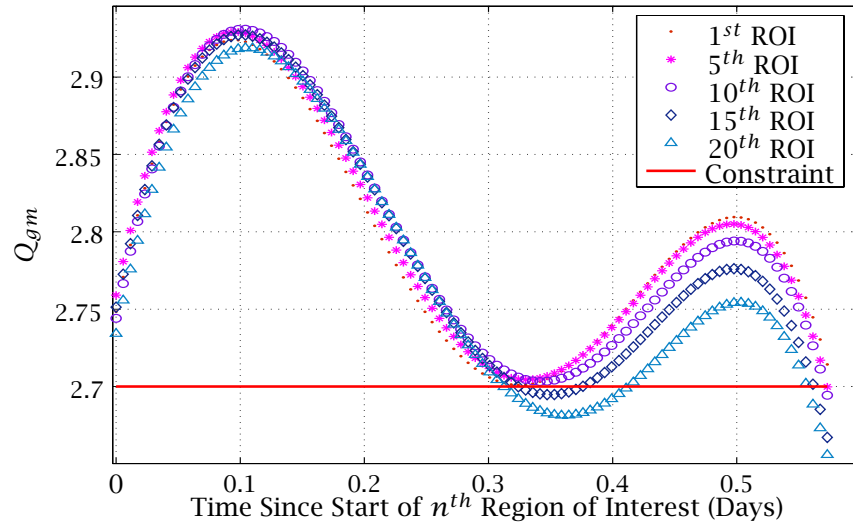


Figure 9: Evolution of Tetrahedral Quality (Q_{gm}) Over Three-Week Period Beyond t_f in Region of Interest for $Q_{\min} = 2.7$.

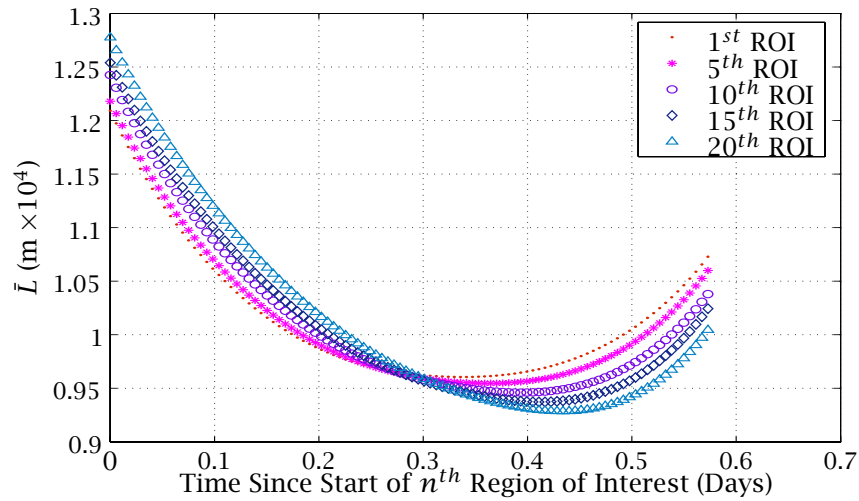


Figure 10: Evolution of Average Length, \bar{L} , Over Three-Week Period After t_f in Region of Interest for $Q_{\min} = 2.7$.

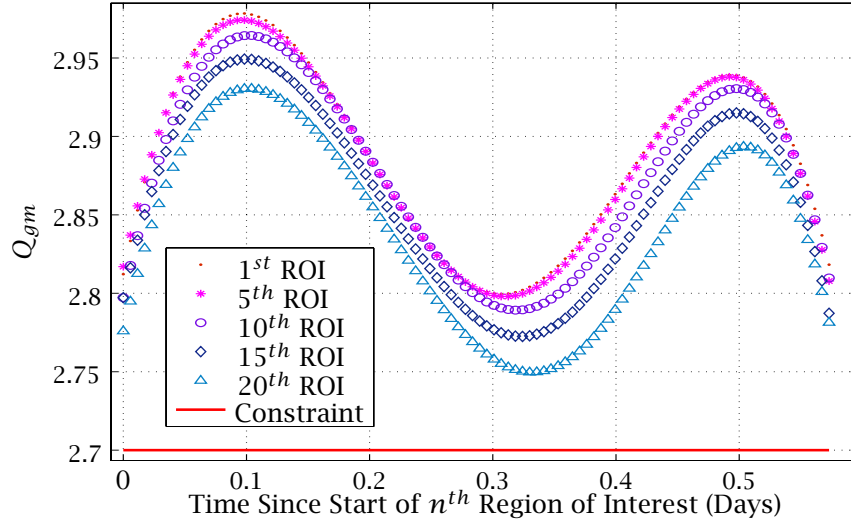


Figure 11: Evolution of Quality Factor, Q_{gm} , Over Three-Week Period After t_f in Region of Interest for $Q_{\min} = 2.8$.

quality factor also degrades (from 2.8) over the three-week period, this time the value of Q_{gm} remains above 2.7 for the entire three week period. However, because of the tighter constraint on Q_{gm} , the amount of fuel burned is significantly greater than the $Q_{\min} = 2.7$ case. In particular, the total fuel burned in the solution to the modified problem was 0.1674 kg (an increase roughly 29% over the 2.7 case). The propellant used by each spacecraft is shown in Fig. 12. In the optimal solution of the modified problem, all four spacecraft utilize two maneuver opportunities, as opposed to the 2.7 case where only one spacecraft burned twice. The phase durations (and consequently the maneuver durations) are shown in Table 10.2. In terms of the terminal tetrahedral formation, the geometry is similar, with some small changes in the relative positions. Fig. 13 directly compares the geometries of the solutions obtained from the 2.7 and 2.8 cases.

Table 3: Phase Durations (in minutes) for $Q_{\min} = 2.8$ case

SC num	Burn1	Coast1	Burn2	Coast2	Burn3	Coast3	Coast ROI
1	0	149.150	0.065	424.850	7.209	0	837.300
2	0	184.517	1.008	241.767	1.107	152.867	837.300
3	1.448	155.767	0	88.200	1.556	334.300	837.300
4	0	273.000	1.268	87.35	0.024	219.617	837.300

11 CONCLUSIONS

In this paper, a minimum-fuel trajectory was designed to transfer four spacecraft from a degraded tetrahedral formation into a tetrahedron that satisfied certain geometric quality constraints for a portion of its orbit. This problem was posed as an optimal control problem and was solved via direct transcription using the Gauss pseudospectral method. The final state of the solution was propagated three weeks into the future to examine the potential degradation of the formation. Observing that the formation degraded in an unacceptably short period of time, a modified optimal control problem was posed that provided margin in the quality factor. It was found that the solution to this modified problem satisfied the tetrahedral quality constraints for this entire three week period beyond the final time of the trajectory design. The

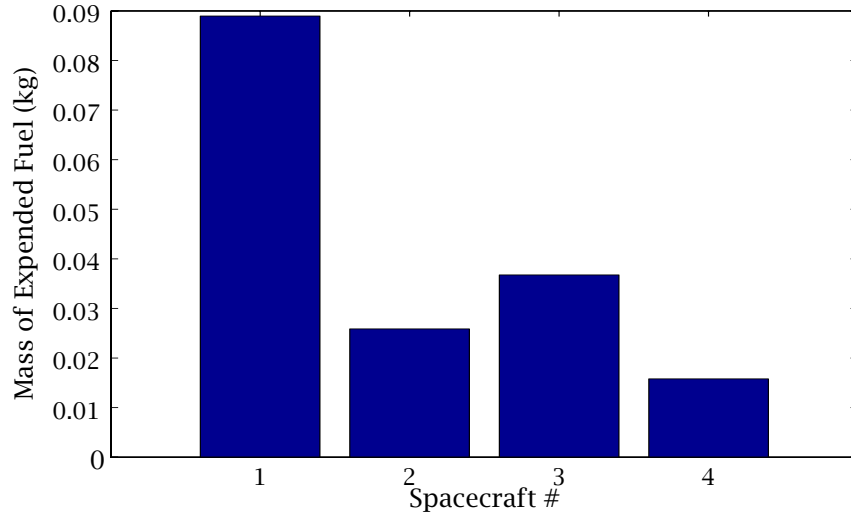


Figure 12: Fuel Expenditure of Each Spacecraft for $Q_{\min} = 2.8$.

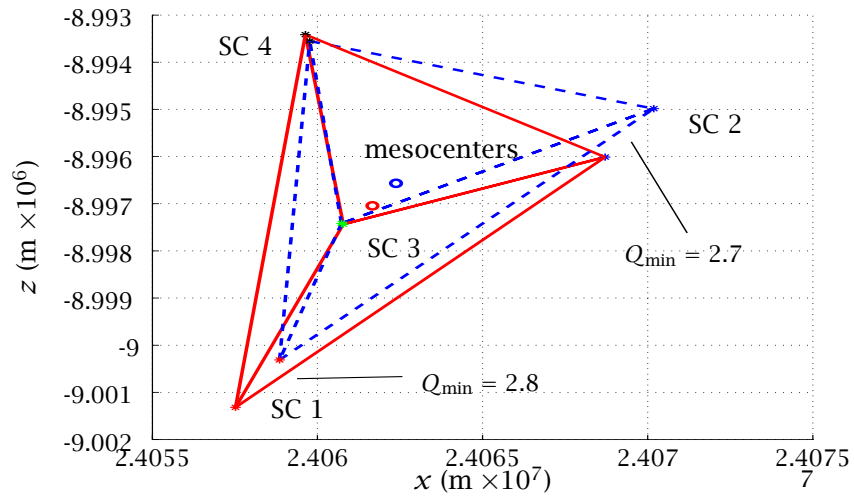


Figure 13: Comparison of Projection of Terminal Tetrahedra into ECI XZ-Plane for $Q_{\min} = 2.7$ and $Q_{\min} = 2.8$.

results in this paper provide insight into the relative motion of tetrahedral formations and demonstrate the applicability of the Gauss pseudospectral method to spacecraft formation flying problems.

ACKNOWLEDGMENT

This work was funded by the NASA Goddard Spaceflight Center under Cooperative Agreement NAS5-NCC5-730. The authors would like to thank Mr. Stephen P. Hughes as technical monitor for his insights and helpful suggestions during the course of this work. The authors would also like to thank Dr. David A. Benson for his help both with the understanding and the implementation of the Gauss pseudospectral method.

APPENDIX: COMPUTATION OF GLASSMEIER QUALITY FACTOR

In order to compute the Glassmeier quality factor at a given point, a few quantities must be calculated. First, using the mesocenter in Eq. (13), the following volumetric tensor is calculated:

$$\bar{\bar{R}}^{I/mc} = \frac{1}{4} \sum_{i=1}^4 \mathbf{r}_{mci} \mathbf{r}_{mci}^T \quad (43)$$

where

$$\mathbf{r}_{mci} = \mathbf{r}^{(i)} - \bar{\mathbf{r}}, \quad i = 1, \dots, 4 \quad (44)$$

Using $\bar{\bar{R}}^{I/mc}$, the volume of the actual tetrahedron is computed as

$$V_a = \frac{8}{3} \sqrt{|\bar{\bar{R}}^{I/mc}|} \quad (45)$$

where $|\bar{\bar{R}}^{I/mc}|$ is the determinant of the volumetric tensor. Next, the surface area of the actual tetrahedron is computed as follows. First, let

$$\begin{aligned} S_1 &= \frac{1}{2} |\mathbf{r}^{(2)} \times \mathbf{r}^{(3)}|, & S_2 &= \frac{1}{2} |\mathbf{r}^{(1)} \times \mathbf{r}^{(3)}|, & S_3 &= \frac{1}{2} |\mathbf{r}^{(1)} \times \mathbf{r}^{(2)}| \\ S_4 &= \frac{1}{2} |(\mathbf{r}^{(2)} - \mathbf{r}^{(1)}) \times (\mathbf{r}^{(3)} - \mathbf{r}^{(1)})| \end{aligned} \quad (46)$$

Then the volume of the actual tetrahedron is given as

$$SA_a = \sum_{i=1}^4 S_i \quad (47)$$

Lastly, the ideal volume and surface area equations are solely a function of the average side length, and are expressed below.

$$V^* = \frac{\sqrt{2}}{12} (\bar{L})^3, \quad SA^* = \sqrt{3} (\bar{L})^2 \quad (48)$$

REFERENCES

1. Scharf, D. P., Hadaegh, F. Y., and Ploen, S. R., "A Survey of Spacecraft Formation Flying Guidance and Control (Part II): Control," *Proceedings of the American Control Conference*, Boston, MA, pp. 2976-2985, 2004.
2. Scharf, D. P., Hadaegh, F. Y., and Ploen, S. R., "A Survey of Spacecraft Formation Flying Guidance and Control (Part I): Guidance," *Proceedings of the American Control Conference*, Denver, CO, pp. 1733-1739, 2003.

3. Guzman, J., Schiff, C., "A Preliminary Study for a Tetrahedron Formation: Quality Factors and Visualization," AIAA Guid, Nav, & Contr, Conf., 2002
4. Hughes, S. "Formation Tetrahedron Design for Phase 1 of the Magnetospheric Multiscale Mission," Flight Dynamics Analysis Branch, NASA Goddard Space Flight Center, 2004.
5. Gim, D. , Alfriend, K. , "Criteria for Best Configuration and Sub-optimal Reconfiguration for MMS Mission," AAS Spaceflight Mechanics Meeting, Maui, HI, Feb. ,2004.
6. Breger, L. ,et. al. , "Distributed Control of Formation Flying Spacecraft Build on OA," AIAA Guidance, Nav, & Control Conference, Austin, TX, Aug 2003.
7. Clemente, D., Atkins, E., "Optimization of a Tetrahedral Satellite Formation," AIAA Guidance, Nav, & Control Conference, Aug 2004.
8. Huntington, G. T., and Rao, A. V., "Optimal Configuration of Spacecraft Formations via a Gauss Pseudospectral Method," *AAS Spaceflight Mechanics Meeting*, AAS 05-103, Copper Mountain, CO, Jan 2005.
9. Mailhe, Laurie M., Guzman, Jose J., "Initialization and Resizing of Formation Flying using Global and Local Optimization Methods," *Proceedings of the IEEE Aerospace Conference*, Big Sky, Montana, paper #1425, 2004.
10. Guzman, Jose J. "Tetrahedron Formation Control," *Journal of the Astronautical Sciences*, Vol. 51, No. 4, pp. 419-431, 2003.
11. Tsuda, Y., "Global Optimization of Maneuver Schedule for Multiple Spacecrafts Flying in Formation," *55th International Astronautical Congress*, Vancouver, Canada, IAC-04-A.2.01, 2004.
12. Betts, J. T., "Survey of Numerical Methods for Trajectory Optimization," *Journal of Guidance, Control, and Dynamics*, Vol. 21, No. 2, 1998, pp. 193-207.
13. Athans, M. and Falb, P. L., *Optimal Control*, McGraw-Hill, New York, 1966, pp. 284-351.
14. Betts, J. T., *Practical Methods for Optimal Control Using Nonlinear Programming*, Society for Industrial and Applied Mathematics Press, 2001.
15. Betts, J. T. and Frank, P. D., "A Sparse Nonlinear Optimization Algorithm," *Journal of Optimization Theory and Applications*, Vol. 82, pp. 519-541, 1994.
16. Gill, P. E., Murray, W., and Saunders, M. A., "SNOPT: An SQP Algorithm for Large-Scale Constrained Optimization," *SIAM Journal on Optimization*, Vol. 12, No. 4, 2002, pp. 979-1006.
17. Hargraves, C. R. and Paris, S. W., "Direct Trajectory Optimization Using Nonlinear Programming and Collocation," *Journal of Guidance, Control, and Dynamics*, Vol. 10, No. 4, 1987, pp. 338-342.
18. Williams, P. , "A Comparison of Differentiation and Integration Based Direct Transcription Methods", AAS/AIAA Space Flight Mechanics Conference, Copper Mountain, CO, Jan. 23-27, 2005. Paper AAS 05-128.
19. Vlases, W. G., Paris, S. W., Lajoie, R. M., Martens, M. J., and Hargraves, C. R., "Optimal Trajectories by Implicit Simulation," Boeing Aerospace and Electronics, Technical Report WRDC-TR-90-3056, Wright-Patterson Air Force Base, 1990.
20. Betts, J. T. and Huffman, W. P., "Sparse Optimal Control Software - SOCS," Mathematics and Engineering Analysis Library Report, MEA-LR-085, Boeing Information and Support Services, P. O. Box 3797, Seattle, WA, 98124-2297, 15 July 1997.
21. Well, K., *Graphical Environment for Simulation and Optimization*, Department of Optimization, Guidance, and Control, Stuttgart, Germany, 2002.
22. Von Stryk, O., "User's Guide for DIRCOL 2.1: A Direct Collocation Method for the Numerical Solution of Optimal Control Problems," Technische Universitat Darmstadt, 1999.
23. Ross, I. M. , "User's Manual for DIDO (Ver. PR.1 β): A MATLAB Application Package for Solving Optimal Control Problems", *Technical Report 04-01.0*, February 2004.
24. Canuto, C., Hussaini, M.Y., Quarteroni, A., Zang, T.A., *Spectral Methods in Fluid Dynamics*, Springer-Verlag, New York, 1988.
25. Elnagar, G. , Kazemi, M. , Razzaghi, M. , "The Pseudospectral Legendre Method for Discretizing Optimal Control Problems," *IEEE Transactions on Automatic Control*, Vol. 40, No. 10, October 1995.
26. Fahroo, F. and Ross, I. M., "Co-state Estimation by a Legendre Pseudospectral Method," *Journal of Guidance, Control, and Dynamics*, Vol. 24, No. 2, March-April 2002, pp. 270-277.
27. Fahroo, F. and Ross, I. M. , "Direct Trajectory Optimization by a Chebyshev Pseudospectral Method," *Journal of Guidance, Control, and Dynamics*, Vol. 25, No. 1, January-February 2002, pp. 160-166.

28. Williams, P. , "Jacobi Pseudospectral Method for Solving Optimal Control Problems", *Journal of Guidance*, Vol. 27, No. 2,2003
29. Williams, P. , "Hermite-Legendre-Gauss-Lobatto Direct Transcription Methods in Trajectory Optimization", AAS/AIAA Space Flight Mechanics Conference, Copper Mountain, CO, Jan 23-27, 2005. Paper AAS 05-131.
30. Rao, A. V. and Clarke, K. A., "Performance Optimization of a Maneuvering Re-entry Vehicle Using a Legendre Pseudospectral Method," *2002 AIAA Atmospheric Flight Mechanics Conference*, AIAA Paper 2002-4885, Monterey, CA August 5-8, 2002.
31. Stanton, S. and Proulx, R., "Optimal Orbital Transfer Using a Legendre Pseudospectral Method," *AAS/AIAA Astrodynamics Specialist Conference*, AAS-03-574, Big Sky, Montana, August 3-7, 2003.
32. Ross, I., King, J., and Fahroo, F., "Designing Optimal Spacecraft Formations," *2002 AIAA/AAS Astrodynamics Specialist Conference*, AIAA Paper 2002-4635, Monterey, CA, August 5-8, 2002.
33. Ross, I. M. and D'Souza, C. , "Hybrid Optimal Control Framework for Mission Planning," *Journal of Guidance, Control, and Dynamics*, Vol. 28, No. 4, July-August 2005.
34. Benson, D., *A Gauss Pseudospectral Transcription for Optimal Control*, Ph.D. Dissertation, Department of Aeronautics and Astronautics, Massachusetts Institute of Technology, November 2004.
35. Wertz, J. R. and Larsen, W. J., *Space Mission Analysis and Design*, 3rd Edition, Microcosm Press, El Segundo, CA and Kluwer Academic Publishers, Dordrecht, The Netherlands, 1999, p. 694.
36. Battin, R. H., *An Introduction to the Mathematics and Methods of Astrodynamics*, AIAA Press, New York, 1987, pp. 490-493 and p. 119.
37. Robert, P., et.al., "Tetrahedron Geometric Factors," *Analysis Methods for Multi-Spacecraft Data* (G. Paschmann and P. Daly, eds.), pp. 323-348, Noordwijk, The Netherlands: ISSI Report SR-001, ESA Publications Division, 1998.
38. Hull, D. G., *Optimal Control Theory for Applications*, Springer-Verlag, New York, 2003.
39. Kirk, D. E. , *Optimal Control Theory*, Prentice-Hall, Englewood Cliffs, NJ, 1970.
40. Gill, P.E., *Users Guide for SNOPT Version 7, A Fortran Package for Large-Scale Nonlinear Programming*, University of California, San Diego, La Jolla, CA, Sept 04.